Polar Gaussian Processes for Predicting on Circular Domains

Espéran Padonou, O Roustant

Polar Gaussian Processes for Predicting on Circular Domains

E. Padonou[a,b,*], O. Roustant[a]

[a]*Mines Saint-Etienne, UMR CNRS 6158, LIMOS, F-42023 Saint-Etienne, France*

[b]*STMicroelectronics, 850 Rue Jean Monnet, 38920 Crolles, France*

Abstract

Predicting on circular domains is a central issue in many industrial fields such as microelectronics and environmental engineering. In this context Gaussian process (GP) regression is used, coupled with Zernike polynomials. However, usual GP models do not take into account the geometry of the disk in their covariance structure (or kernel), which may be a drawback at least for technological or physical processes involving a rotation or a diffusion from the center of the disk. For that purpose, we introduce so-called polar GPs defined on the non-Euclidian space of polar coordinates. Their kernels are obtained as a combination of a kernel for the radius using an Euclidean distance, and a kernel for the angle, based on either chordal or geodesic distances on the unit circle. Their efficiency is illustrated on two industrial applications where radial and angular patterns are visible. In a second time, the problem of defining an initial design of experiment (DoE) for circular domains is considered. Two new Latin hypercube designs are obtained, by defining a valid maximin criterion for polar coordinates. Their robustness in prediction is assessed and compared to other DoEs over a range of various toy functions and models.

Key words: Gaussian process regression, Polar coordinates, Circular domain, Design of Experiments

1. Introduction

This research aims at analyzing costly computer or physical experiments on a disk. The question was motivated by two industrial problems. In semiconductor produc-

*Corresponding author.

Email addresses: esperan.padonou@st.com (E. Padonou), roustant@emse.fr (O. Roustant)

tion plants first, integrated circuits are produced on disks called wafers. Several technological processes, such as lithography, heating or polishing, exploit the geometry of the disk, involving rotations or diffusions from the center. A common issue is to reconstruct a quantity of interest over the whole disk, from few measurements at specific locations. The second problem is related to air pollution modelling for environmental impact assessment. Greenhouse gas concentrations are simulated by a computer code. Among the input variables, the couple (speed, direction) of wind characteristics can be represented on a disk, the radius of which corresponds to the maximal speed. Here also, the goal is to predict the gas concentration from some simulated experiments.

Approximation problems on the disk have been considered since the works of Zernike [1] in optics. Zernike polynomials are orthogonal with respect to the usual scalar product on the unit disk, a useful property for linear models. For such models, optimal design of experiments are known to be included in concentric circles [2]. More recently, a stochastic model consisting of a Gaussian process (GP), also called Kriging model, has been proposed for microelectronics applications [3]. However its covariance kernel, often simply called kernel hereafter, does not take into account the geometry of the disk, which may be a drawback, at least for technological or physical processes involving a diffusion from the center of the disk, or a rotation. Indeed the prediction of a GP model is weighting more importantly the observed values corresponding to neighboring locations. With usual GPs, the neighbors are computed with respect to the Euclidian distance, which underestimates the influence of points located on same concentric circles.

The main aim of the paper is to propose GP models that incorporate the geometry of the disk in their covariance kernel. For that purpose, we consider the parametrization of the unit disk in polar coordinates: $\mathcal{D} = \{(\rho\cos\theta, \rho\sin\theta), \rho \in [0,1], \theta \in \mathbb{S}\}$ where $\mathbb{S}$ represents the unit circle $\mathbb{R}/2\pi\mathbb{Z}$. The idea is to define a GP on the parametrization space $\mathcal{C} =]0,1] \times \mathbb{S}$ defined by (ρ, θ). This implies constructing a kernel on a product of the Euclidian space $]0,1]$ and on the circle $\mathbb{S}$, which can be done by algebraically combining kernels on these two spaces with sum, product or ANOVA operations for instance. The corresponding GPs will be called here *polar* GPs, and the usual ones based on Cartesian coordinates, *Cartesian* GPs.

The construction of kernels on $\mathbb{S}$ can be achieved in several ways, and is connected to the literature of directional data (see e.g. [4, 5]) and periodic functions (see e.g. [6]). One possibility is to use so-called wrapped GP [7], obtained by transforming a multinormal density to a periodic one by applying an operator written as an infinite sum. Here we focus on simpler approaches that provide explicit kernel expressions,

either by considering restriction to $\mathbb{S}$ of a 2-dimensional GP [6], involving the chordal distance on $\mathbb{S}$, or by using the recent results of Gneiting [8], involving the geodesic distance on $\mathbb{S}$. The geodesic distance on a general manifold was used recently by del Castillo et al. [9] in the context of free-form monitoring, with so-called geodesic GPs. However, the goal and the approach are quite different here, where the form is fixed (the unit disk) and the geodesic distance known analytically. Furthermore, here the geodesic is relative to the manifold $\mathbb{S}$ which is only an algebraic portion of the mapped space $\mathcal{C}$.

In a second time, we address the issue of defining an initial design of experiments (DoE) for circular domains. Considering the space $\mathcal{C}$ of polar coordinates is natural, but standard designs cannot be used directly due to its non-Euclidian structure. By considering a valid distance, we obtain maximin Latin hypercube designs (LHD, [10]) on $\mathcal{C}$. That class of designs is recommended when the process has a physical interpretation in polar coordinates. In order to deal with more general situations, we also propose a modified version, which still has the LHD structure with respect to ρ and θ, and is well filling the disk $\mathcal{D}$.

The paper is organized as follows. Section 2 presents the background and fixes notations. Section 3 introduces so-called polar GPs. Section 4 shows the strength of the approach on two real applications, in microelectronics and environments. Section 5 is devoted to designs of experiments. Two new LHDs are introduced and compared to common designs, with respect to quality criteria. Their robustness in prediction is also investigated on a set of toy functions and models. Section 6 discusses the range of applicability of polar GPs and gives perspectives for future research.

2. Background and notations

Denote $\mathcal{D}$ the unit disk represented either in Cartesian or polar coordinates:

$$\mathcal{D} = \{(x, y) \in \mathbb{R}^2, x^2 + y^2 \leq 1\} = \{(\rho\cos\theta, \rho\sin\theta), \rho \in [0, 1], \theta \in \mathbb{S}\}$$

where $\mathbb{S} = \mathbb{R}/2\pi\mathbb{Z}$ is the unit circle. In various situations, one has to predict a variable of interest which is measured at a limited number of locations in $\mathcal{D}$. For that purpose, we will consider the framework of Gaussian Process Regression (GPR) [6] also called Kriging in reference to its origins in geostatistics (see e.g. [11]). The measurement locations, also called design points, will be denoted by $X = \left(\mathbf{x^{(1)}}, \ldots, \mathbf{x^{(n)}}\right)$. In GPR, the observed values at X are modeled by:

$$Y_i = \mu(\mathbf{x^{(i)}}) + Z(\mathbf{x^{(i)}}) + \eta_i \tag{1}$$

where μ is a trend function, $Z \sim GP(0, k)$ is a centered Gaussian process (GP) with covariance function – or *kernel* – k, and $\eta_1, \ldots, \eta_n$ are Gaussian random variables representing noise. We now briefly detail the three parts of the model.

The trend function μ is deterministic and often modeled as a linear combination of basis functions:

$$\mu(\mathbf{x}) = \mathbf{f}(\mathbf{x})^\top \boldsymbol{\beta}$$

where $\boldsymbol{\beta}$ is a vector of unknown coefficients. In our situation, Zernike polynomials [1] are good candidates for basis functions since they constitute an orthogonal basis for the usual scalar product restricted to $\mathcal{D}$. Their shape including regular patterns are also suited to describe symmetries or rotations, and have been recently used for predicting on a disk by Pistone and Vicario [3].
The stochastic part of model 1 comprises a GP and a noise. The GP Z takes into account the spatial dependence, which thus entirely depends on its kernel k. The choice of k is crucial for applications, and may be done in order to include knowledge such as smoothness, periodicity, symmetries, etc. There are many ways to construct a kernel, and a comprehensive presentation is found in [6], Section 4. A key idea is that multidimensional kernels can be obtained by algebraic operations, such as sum or products, of 1-dimensional kernels.
Finally the noise part represented by the η_i's may have two different purposes: Modelling a measurement noise, or adding flexibility. In this paper we assume that the η_i's are independent $N(0, \tau^2)$, where τ^2 is an unknown homogeneous variance term often called "nugget". When conditioning by the observed values, the model will interpolate the observations if $\tau = 0$ but not if $\tau > 0$, which gives more flexibility.

When all parameters are known, prediction with Equation (1) is given in a closed form by a Gaussian conditional distributions knowing the observations Y_i, $i = 1, \ldots, n$. Its two moments are known as Kriging mean and Kriging variance. Analytical expressions are also available when the parameters are estimated, known as universal Kriging formulas (see e.g. [6] for more details), that we use here. An important fact is that the Kriging mean at a new site $\mathbf{x}$ is obtained as an affine combination of the observed values Y_i, with weights depending on $k(\mathbf{x}, \mathbf{x}^{(i)})$. Since k corresponds to the spatial dependence, the weights are more important for the $\mathbf{x}^{(i)}$'s that are close to $\mathbf{x}$ when this vicinity is measured by k.

3. Polar Gaussian processes

One way to define a GP on the unit disk $\mathcal{D}$ is to use the restriction of a GP on the square $[0,1]^2$, defined in Cartesian coordinates. In this paper, we will call them *Cartesian* GPs. Here, we propose to further exploit the geometry of the disk by using the polar coordinates. The associated GPs will be callled *polar* GPs.

When using the polar coordinates, the unit disk $\mathcal{D}$ is connected to the cylinder $\mathcal{C} =]0,1] \times \mathbb{S}$, where $\mathbb{S}$ denotes the unit circle, with the mapping, also called warping in the context of GP modeling (see e.g. [6], Section 4.2.3.):

$$\Psi : (\rho, \theta) \in \mathcal{C} \mapsto (\rho \cos\theta, \rho \sin\theta) \in \mathcal{D} \setminus \{\mathbf{0}\} \tag{2}$$

This mapping is a one-to-one correspondence from $\mathcal{C}$ to the unit disk without its center. The fact that the center is lost in the mapping may be a problem in theory. In practice a design point located at the center of the disk can be replaced by a set of design points placed on a closed concentric circle. A GP on $\mathcal{D}$ can then be obtained by using Ψ^{-1}, resulting in kernels on $\mathcal{D} \times \mathcal{D}$ of the form:

$$k(\mathbf{x}, \mathbf{x}') = k_{\mathcal{C}}\left(\Psi^{-1}(\mathbf{x}), \Psi^{-1}(\mathbf{x}')\right) \tag{3}$$

where $k_{\mathcal{C}}$ is a kernel on $\mathcal{C} \times \mathcal{C}$.

Kernels on the cylinder can be defined by exploiting its product structure. This can be done by combining a kernel k_{r} on $]0,1]\times]0,1]$ and a kernel k_{a} on $\mathbb{S} \times \mathbb{S}$. A first way is by using the tensor product:

$$k_{\mathrm{prod}}\left(\mathbf{u}, \mathbf{u}'\right) = k_{\mathrm{r}}\big(\rho, \rho'\big) k_{\mathrm{a}}\left(\theta, \theta'\right) \tag{4}$$

where $\mathbf{u} = (\rho, \theta)$ and $\mathbf{u}' = (\rho', \theta')$ are in $\mathcal{C}$. This formulation implicitly assumes that $Z_{\mathbf{u}}$ is the product of two independent components: a radial process R_ρ and an angular process A_θ ($Z_{\mathbf{u}} = R_\rho A_\theta$). It corresponds to a simple form of interaction. For processes that do not have interactions between these components ($Z_{\mathbf{u}} = R_\rho + A_\theta$), an additive kernel should be more appropriate:

$$k_{\mathrm{add}}\left(\mathbf{u}, \mathbf{u}'\right) = k_{\mathrm{r}}\big(\rho, \rho'\big) + k_{\mathrm{a}}\left(\theta, \theta'\right) \tag{5}$$

A trade-off between these two extreme approaches is the ANOVA kernel defined as:

$$k_{\mathrm{ANOVA}}\left(\mathbf{u}, \mathbf{u}'\right) = \Big(1 + k_{\mathrm{r}}\big(\rho, \rho'\big)\Big)\Big(1 + k_{\mathrm{a}}\left(\theta, \theta'\right)\Big) \tag{6}$$

The expanded form of Equation (6) shows that a process $Z_{\mathbf{u}}$ with ANOVA kernel can be viewed as a sum of four independent GPs: a constant process Z^0, a radial process R_ρ with kernel k_{r}, an angular process A_θ with kernel k_{a}, and a process Z^{inter} on $\mathcal{C}$ with kernel $k_{\mathrm{r}}k_{\mathrm{a}}$. From the ANOVA point of view, these processes are similar to constant term, main effects, and second-order interaction [12], but without respecting the unicity constraints such as centering. Though out of the scope of this paper, a so-called KANOVA kernel mimicking exactly the ANOVA decomposition could have been proposed [13]. For more details on how to make new kernels from old, we refer the reader to [6].

Let us now define the kernels k_{r} on $]0,1]\times]0,1]$ and k_{a} on $\mathbb{S}\times\mathbb{S}$. We recall that valid kernels must be positive definite. The domain $]0,1]$ is a segment of a 1-dimensional Euclidean space. As a consequence, traditional kernels are suitable for k_{r}. In particular, Matérn kernels are attractive for their ability to control the smoothness of the process and to ensure numerical stability. In dimension 1, the Matérn $\frac{5}{2}$ kernel is given by:

$$k_{\mathrm{m}}(x,x') = \left(1 + \frac{\sqrt{5}\mid x-x'\mid}{\ell} + \frac{5(x-x')^2}{3\ell^2}\right)\exp\left(-\frac{\sqrt{5}\mid x-x'\mid}{\ell}\right) \tag{7}$$

A simple way of defining kernels on $\mathbb{S}\times\mathbb{S}$ is mentioned by Gneiting [8]. They are based on the chordal distance $d_1(\theta,\theta') = 2\sin\left(\frac{\theta-\theta'}{2}\right)$ and the geodesic distance $d_2(\theta,\theta') = \mathrm{acos}\big(\cos(\theta-\theta')\big)$ illustrated in Figure 1.

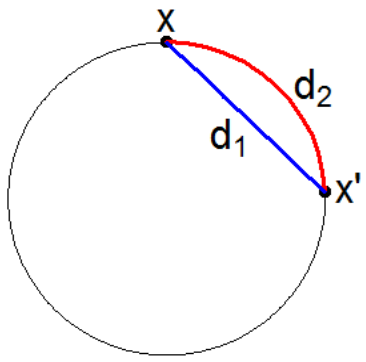

Figure 1: Chordal (d_1) and geodesic (d_2) distances on $\mathbb{S}$.

To define a kernel on $\mathbb{S}\times\mathbb{S}$, one could be tempted to apply usual kernels to d_1 or d_2. Unfortunately, positive definiteness is not guaranteed for the resulting functions

when d_2 is used. As a counter-example, if the Gaussian kernel is chosen for k_{a}, then $k_{\mathrm{a}} \circ d_2$ is not positive definite ([8], Th. 8). Two sufficient conditions are given in [8] :

(i). If $h : [0, \infty) \to \mathbb{R}$ is a kernel, then $h \circ d_1$ is a kernel on $\mathbb{S} \times \mathbb{S}$

(ii). If in addition $h(t) = 0$ for $t \geq \pi$, then $h \circ d_2$ is a kernel on $\mathbb{S} \times \mathbb{S}$

Kernels satisfying (i) were initially proposed by Yadrenko in 1983 [8] and are often used to describe periodic functions [6]. They correspond to restrictions of 2-dimensional isotropic GPs on $\mathbb{R}^2$ to $\mathbb{S}$. Kernels satisfying (ii) can be constructed from compactly supported functions on $\mathbb{R}$ such as the C^2-Wendland function defined for $0 \leq t \leq \pi$:

$$W_c(t) = \left(1 + \tau \frac{t}{c}\right) \left(1 - \frac{t}{c}\right)_+^{\tau}, \qquad c \in]0, \pi]; \tau \geq 4 \tag{8}$$

For the geodesic distance, we use $c = \pi$, which is the largest possible value due to condition (ii) above. With this choice, the covariance between two angles θ, θ' is zero when $d_2(\theta, \theta') = \pi$, and strictly positive for $d_2(\theta, \theta') < \pi$. The same interpretation is possible for the chordal distance with $c = 2$, though it is not necessary to use a compactly supported function in that case. From now on, we will use the Wendland function in both cases, resulting in the two following kernels on $\mathbb{S} \times \mathbb{S}$:

$$k_{\mathrm{chord}}(\theta, \theta') = W_2(d_1(\theta, \theta')), \tag{9}$$

$$k_{\mathrm{geo}}(\theta, \theta') = W_\pi(d_2(\theta, \theta')), \tag{10}$$

and the corresponding GPs will be denoted *polar GP (chordal)* and *polar GP (geodesic)*.

GP simulations on the unit disk

In order to have a first contact with polar GPs, it is useful to draw simulated surfaces. For the sake of simplicity, we propose to focus on the ANOVA combinations. We consider a Cartesian GP and the two polar GPs (chordal, geodesic) defined in Equations (9), (10). Their expressions are written below, including variance factors s^2, α_1^2, α_2^2:

(a) $k(\mathbf{x}, \mathbf{x}') = s^2 \Big(1 + \alpha_1^2 \, k_{\mathrm{m}}\big(x, x'\big)\Big) \Big(1 + \alpha_2^2 \, k_{\mathrm{m}}(y, y')\Big)$

(b) $k(\mathbf{x}, \mathbf{x}') = s^2 \Big(1 + \alpha_1^2 \, k_{\mathrm{m}}\big(\rho, \rho'\big)\Big) \Big(1 + \alpha_2^2 \, k_{\mathrm{chord}}(\theta, \theta')\Big)$

(c) $k\left(\mathbf{x},\mathbf{x}'\right)=s^2\Big(1+\alpha_1^2\,k_{\mathrm{m}}\big(\rho,\rho'\big)\Big)\Big(1+\alpha_2^2\,k_{\mathrm{geo}}\left(\theta,\theta'\right)\Big)$

Simulation results are displayed in Figure 2. We can see that with polar GPs, the simulated surface exhibits radial and angular patterns around the center of the disk. Such kernels may thus be suitable to describe physical phenomena involving such effects. Figure 3 shows via Kriging standard deviation how model uncertainty varies over $\mathcal{D}$, given a design of 17 points. Two striking differences are visible, especially between the Cartesian GP and the polar GP (geodesic), about uncertainty at the center of the disk, and uncertainty regions at the vicinity of design points. On one hand, the neighborhoods produced by the Cartesian GP look lie elliptical regions at any location of the circular domain. On the other hand, those produced by the polar GP (geodesic) look like pie chart sectors oriented towards the center of the disk, which plays a particular role. This is also true for the polar GP (chordal), though less pronounced.

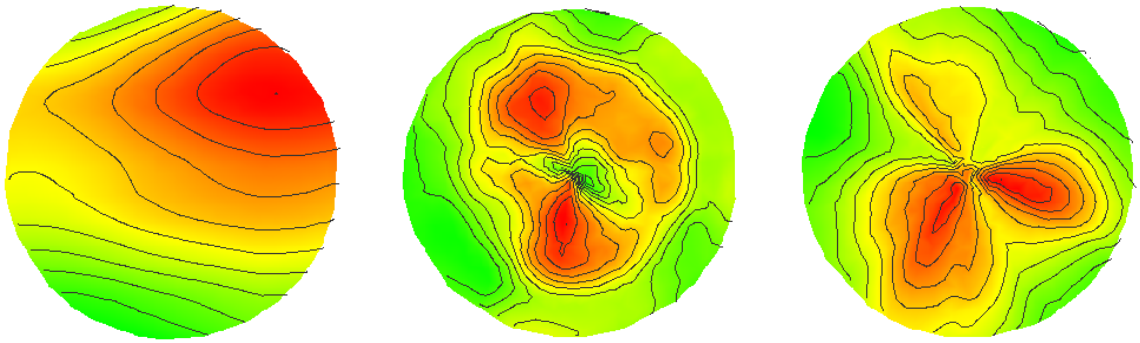

Cartesian GP | Polar GP (chordal) | Polar GP (geodesic)

Figure 2: Simulations of Cartesian and polar GPs with kernels (a)-(c).

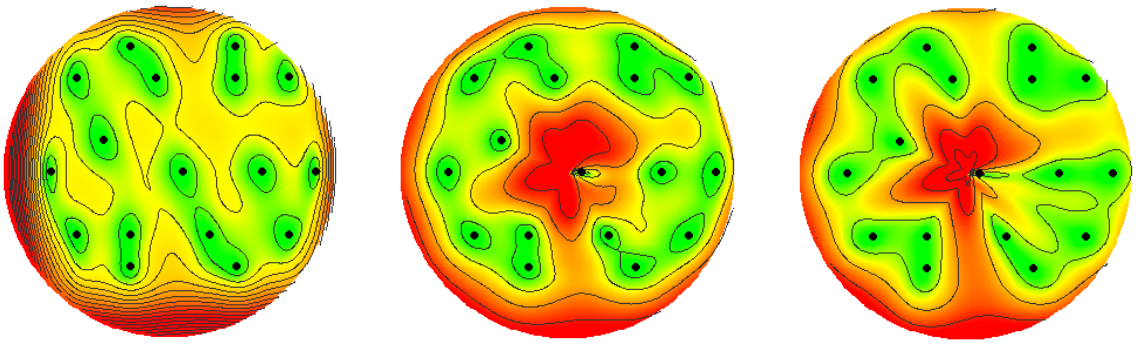

Cartesian GP | Polar GP (chordal) | Polar GP (geodesic)

Figure 3: Kriging standard deviations for Cartesian and polar GPs (kernels (a)-(c))

4. Applications

4.1. Quality control in microelectronics

In microelectronics, integrated circuits are produced on circular slices of semiconductor materials called wafers. For quality monitoring, physical and electrical variables are collected on a set of locations of these wafers. A statistical challenge consists in predicting non measured-points in order to assess the spatial risk of default. In our industrial background, thickness is measured at only 17 points of a wafer for economical reasons. Exceptionally, for the purpose of this study, thickness is further measured at 64 new locations to serve as a test grid. For the sake of confidentiality, the thickness values have been rescaled. For the same reason the technological process is not detailed. It produces here data with a pronounced radial pattern.

The aim of this section is to compare the Cartesian and polar GPs (chordal, geodesic), obtained with 3 types of algebraic combination (product, sum, ANOVA). The Cartesian GPs considered here are obtained by tensor product, tensor sum or ANOVA product of the 1-dimensional Matérn kernel of Equation (7). For the polar GPs, we use the same combinations for a kernel k_{r} on $]0,1]$ and a kernel k_{a} on $\mathbb{S}\times\mathbb{S}$, accordingly to Equations (4), (5), (6). For k_{r}, we use again the Matérn kernel, whereas for k_{a} we choose k_{chord} or k_{geo} (see Equations (9), (10)). The parameters are estimated by maximum likelihood with R package GPlab [14]. The model accuracy is computed on the 64 test points, with the root mean squared error (RMSE) criterion. The results are summarized in Table 1 when a constant trend is used for μ in Equation 1. They show that the smallest prediction errors are obtained with the polar GPs,

corresponding to gains around 20% compared to the Cartesian GP. Adding Zernike polynomials as a trend slightly improves the result for the Cartesian GP, but the untrended polar GPs still outperform with a gain of 15%. Actually the trend captures the main part of the phenomenon and the GP part has then a minor effect: results are the same as for a pure linear model based on Zernike polynomials of order 2.

In order to further analyze the results, we select for each GP type the kernel corresponding to the best combination, repaired by an asterisk in Table 1. The prediction surfaces obtained with these 3 kernels are shown on Figure 5. All the GPs succeed in recovering the radial pattern of the dataset, visible on Figure 4, middle. However, it is less faithfully identified by the Cartesian GP, though the radial property is detected by estimation: Indeed its kernel approximately depends on $\left(\frac{x-x'}{\ell_1}\right)^2 + \left(\frac{y-y'}{\ell_2}\right)^2$, and the estimated values of ℓ_1, ℓ_2 are close (0.6 and 0.8). To understand the difference on the predicted values, recall that they weight more importantly the observed values corresponding to neighboring locations. With the Cartesian GP, the neighbors are the closest locations whereas with polar GPs they also involve other locations such as those placed on same concentric circles. Thus the predicted values of the bottom right region are larger for the polar GPs, since the thickness values at the boundaries of the disk are larger than in the middle. Finally notice that the predicted value at the extreme boundary of the disk should be considered with care, since no test points are defined on this region due to technical constraints.

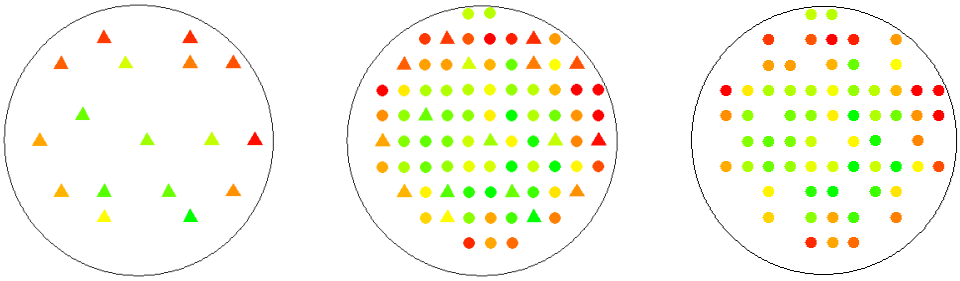

Design points Design and test points Test points

Figure 4: Color representation of thickness values. The 81 measurement locations are shown in the middle, including 17 design points (triangles, left) and 64 test points (bullets, right).

GP type	Cartesian			Polar (chordal)			Polar (geodesic)		
Kernel type	k_{prod}	k_{add}	k_{ANOVA}	k_{prod}	k_{add}	k_{ANOVA}	k_{prod}	k_{add}	k_{ANOVA}
RMSE	0.75 *	0.77	0.76	0.69	0.60 *	0.62	0.68	0.61 *	0.65

Table 1: RMSE computed on 64 test points for several GPs with a constant trend. For each GP type, the combination resulting in the smallest RMSE is marked by an asterisk. When a Zernike trend is added, the best RMSE is equal to 0.71 for all GP types, corresponding to the score of the linear trend only.

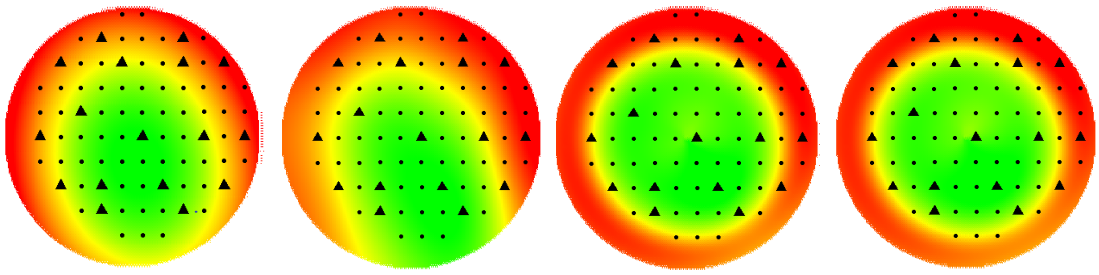

Zernike regression Cartesian GP Polar GP (chordal) Polar GP (geodesic)

Figure 5: Prediction surface for the best untrended GP models of Table 1. When adding a Zernike trend, the prediction surface is approximately the same as for a pure Zernike regression represented on the left. Black bullets correspond to test points, triangles to design points.

4.2. Air pollution modelling with a directional input

The problem tackled here is a an environmental question. A greenhouse gas emitted by a known source, usually an industrial plant, is measured at a given location for air quality monitoring. In the absence of sensors, gas concentration must be predicted. For simple landscapes, analytical expressions are available based on transport and diffusion equations. However, for complex landscapes, gas concentration is simulated by numerical codes [15]. The input variables include the emitted flow, landscape characteristics and meteorological variables. Here we focus on wind speed and wind direction. In this short study, 242 simulations were carried out, 30 of which serve as design points and the other ones are used for tests, as illustrated in Figure 6. The wind speed, initially given on the range $[0; 12]$ $(m.s^{-1})$, is rescaled to $[0, 1]$. With this transformation, the domain of the variables (speed, direction) is the unit disk.

The aim of this study is simply to compare the prediction accuracy of Cartesian and

polar GPs, without using a priori information. In particular, we do not specify the constraints of positivity or nullity of the gas concentration on a known subregion. We use the same kernels as in the first application, corresponding to 3 algebraic combinations (product, sum, ANOVA). Here, the best model is obtained for the tensor-product combination for all kinds of GPs. This claims in favor of an interaction speed-direction for the wind on gas concentration. Notice that adding a Zernike polynomial trend does not improve the results here, since the angular shape is restricted to a region of the disk, which is hard to capture with Zernike polynomials. The results are displayed in Figure 7. In terms of prediction accuracy (measured by the RMSE criterion) the polar GPs are clearly outperforming, corresponding to gains around 40% compared to the standard tensor-product Matérn kernel. Furthermore, for the polar GPs the influence of wind direction on gas concentration has an angular shape, which is intuitive, and corresponds to the true shape visible in Figure 6 (middle). On the other hand, this shape is rectangular for the Cartesian GP.

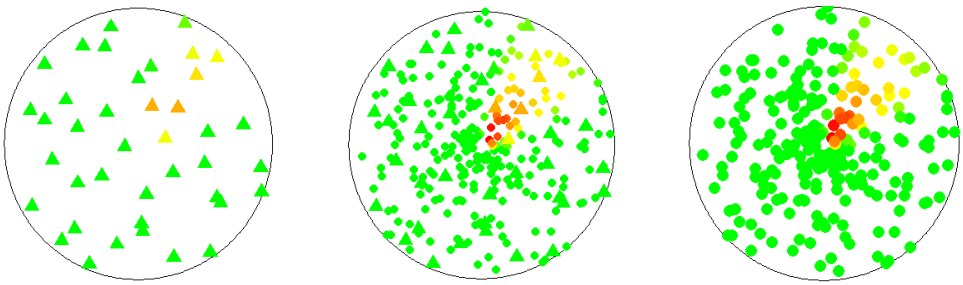

Design points. Design and test points. Test points.

Figure 6: Color representation of gas concentrations. The 242 simulation locations are shown in the middle, including 30 design points (triangles, left) and 212 test points (bullets, right).

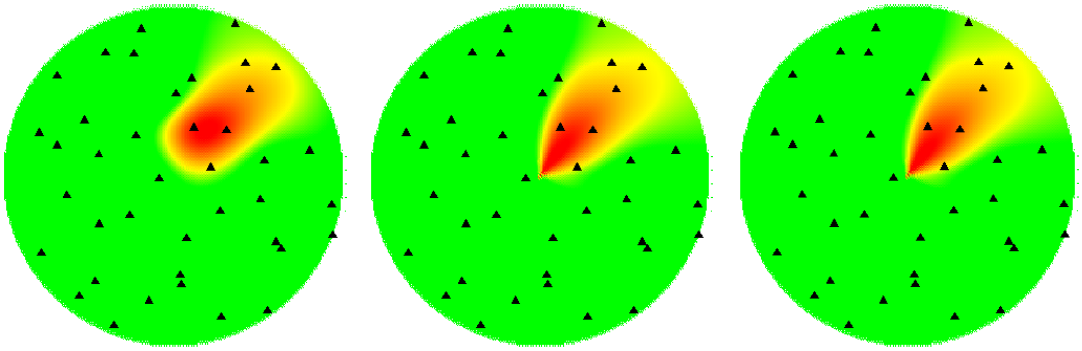

Cartesian GP
RMSE = 0.61

Polar GP (chordal)
RMSE = 0.38

Polar GP (geodesic)
RMSE = 0.37

Figure 7: Estimated gas concentrations according to wind speed (ρ) and direction (θ), for untrended Cartesian and polar GPs. Adding a Zernike polynomial trend does not improve the results. Triangles correspond to design points.

5. Design of experiments on the disk

5.1. Optimal designs for Zernike polynomials and spirals

Among the DoEs that are specific to the disk, there are optimal designs for Zernike polynomials. The D-optimal designs were investigated by [2] and were found to be contained in few concentric circles, as illustrated in Figure 8.
Spirals, hereafter denoted spiral DoEs, are used in various industrial settings: Microelectronics, optics, microbiology, etc. They allow to control the density of the design [16]. Some of them are represented in Figure 9, corresponding to the equation $\rho = a\theta^p + b$.

Some issues arise from these two classes of DoEs. D-optimal DoEs for regression models are not robust to departures from the assumed shapes [17], and do not fill the space, a property usually required in the framework of GP modelling for capturing potential non-linearities. Poor space-filling properties are also visible for spirals in the space (ρ, θ) of polar coordinates, as shown in Figure 10, though they may correctly fill the disk.

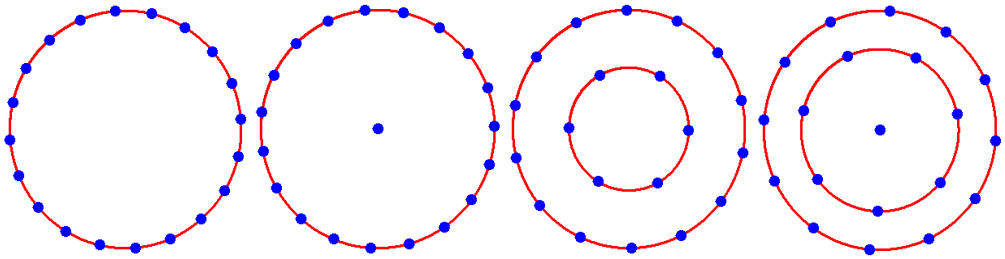

Figure 8: 20-point D-optimal DoEs for Zernike polynomials of degree N.

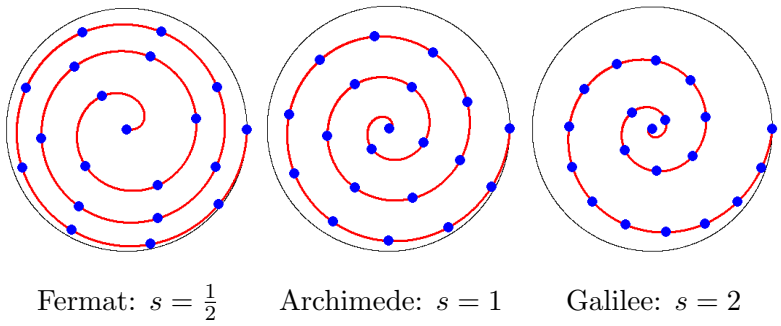

Figure 9: 20-point DoEs defined from spirals of the form $\rho = a\theta^s + b$ with $\theta \in [0, 6\pi]$. The parameter s controls the speed with which the curve moves away from the center, and a, b are chosen such that the spirals start at the center and end at the boundary.

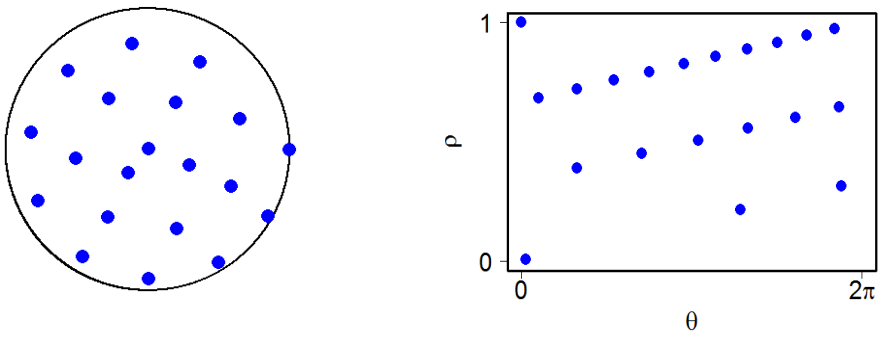

Figure 10: Cartesian (left) and polar (right) representations of the Archimedean spiral DoE. This DoE is filling well the disk but not the cylinder of polar coordinates.

5.2. Maximin Latin hypercubes for polar coordinates.

For metamodelling a potentially complex phenomenon, two main properties are expected from a good DoE: Space-filling, in order to capture non-linearities, and uniformity of the marginal distributions, to avoid redundancies in projection. Among the indicators used to assess space-fillingness, the maximin criterion [18] is a common choice. In addition, Latin hypercube designs (LHD, [10]) provide good projection properties onto marginal dimensions. Thus, maximin LHDs are often proposed as initial DoEs. However such designs cannot be directly used in polar coordinates, due to the non-Euclidian structure of $\mathcal{C}$. To adapt their construction is the aim of this section.

Let us first recall the construction of a maximin LHD over the hypercubic domain $[0,1]^2$. Given a design $\mathbf{X} = \left(\mathbf{x^{(1)}}, \ldots, \mathbf{x^{(n)}}\right)$ of elements of $[0,1]^2$, we denote $\Phi_{\text{Mn}}(\mathbf{X})$ the so-called maximin criterion, giving the minimal distance among design points:

$$\Phi_{\text{Mn}}(\mathbf{X}) = \min_{i \neq j} \left(\| \mathbf{x^{(i)}} - \mathbf{x^{(j)}} \| \right) \tag{11}$$

A maximin DoE is a design that maximizes Φ_{Mn}. However, Φ_{Mn} is hard to optimize and [19] proposed a regularized version ϕ_p, more suitable for optimization:

$$\phi_p(\mathbf{X}) = \left(\sum_{1 \leq i < j \leq n} \| \mathbf{x^{(i)}} - \mathbf{x^{(j)}} \|^{-p} \right)^{\frac{1}{p}} \tag{12}$$

For $p \to \infty$, maximizing Φ_{Mn} is equivalent to minimizing ϕ_p. Following [19, 20], we will use $p = 50$. In softwares, the algorithms used for optimization are often based on simulated annealing or evolutionary strategies (see e.g. [21]).

Now let us consider the cylinder $\mathcal{C}$ of polar coordinates. The construction of a Latin hypercube on $\mathcal{C}$ is identical for an hypercubic domain, by considering discretizations of $[0,1]$ and $\mathbb{S}$. However, the maximin criterion must be adapted to a valid distance on $\mathcal{C}$, ensuring that $\| \mathbf{u} - \mathbf{u}' \| = 0$ for $\mathbf{u} = (\rho, \theta)$ and $\mathbf{u}' = (\rho, \theta')$, with $\theta = \theta' \pmod{2\pi}$. In particular the Euclidian distance is not further valid, since it does not see that the points $(\rho, 0)$ and $(\rho, 2\pi)$ are the same in $\mathcal{C}$. Valid distances on $\mathcal{C}$ can be obtained by combining distances on $]0,1]$ and $\mathbb{S}$. We propose to consider the following distance:

$$\| \mathbf{x} - \mathbf{x}' \|_{\text{Polar}} = \sqrt{(\rho - \rho')^2 + \left(\frac{d_2(\theta, \theta')}{\pi} \right)^2} \tag{13}$$

The factor $\frac{1}{\pi}$ rescales d_2 to $[0,1]$ in order to weight equivalently radius and angle.

From now on we will denote Φ_{Polar} (resp. $\Phi_{\text{Cartesian}}$) the Φ_p criteria computed with $\| \cdot \|_{\text{Polar}}$ (resp. $\| \cdot \|_2$). Minimizing Φ_{Polar} leads to a maximin LHD according to (ρ, θ). A 20-point maximin LHD is displayed in Figure 11, where the cylinder is represented as a 2-dimensional map. As expected it is well filling the space of polar coordinates. Though it looks similar to a maximin LHD obtained in an hypercubic domain with the usual Euclidian distance, the difference is visible on the left and right boundaries which correspond to the same points in $\mathcal{C}$: the design points near the left and right boundaries are also spread out from each other.

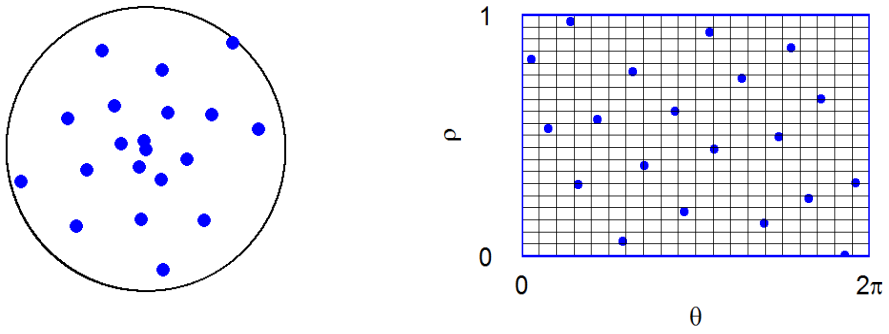

Figure 11: Cartesian (left) and polar (right) representations of a 20-point maximin LHD. The design is well-filling the cylinder $\mathcal{C}$ of polar coordinates, displayed as a 2-dimensional map: In particular, the design points near the left and right boundaries are also spread out from each other.

The LHDs constructed on $\mathcal{C}$ are recommended when the studied phenomenon has a physical interpretation with respect to polar coordinates. First, if the phenomenon is purely radial (resp. angular), the Latin hypercube structure ensures that all the design radius (resp. angles) values are different, so that no information is lost by projection. Furthermore, the maximin property helps in capturing non-linearities with respect to ρ and θ. However, when no a priori information about the phenomenon is known, the maximin LHDs on $\mathcal{C}$ may be inappropriate, due to non-uniform filling that they produce on $\mathcal{D}$, as visible in Figure 11.

Though it is not possible to optimize simultaneously maximin criteria based on distances in Cartesian and polar coordinates, a multi-criteria approach could have been investigated. In this paper, as a first study, we focus on a simple transformation of a maximin LHS on $\mathcal{C}$ which helps improving space-fillingness on $\mathcal{D}$ while preserving the Latin hypercube structure on $\mathcal{C}$. This is done by applying the transform $\rho \mapsto \sqrt{\rho}$, based on the well-known fact that if R is a uniform random variable on $[0, 1]$ and T is

uniform on $[0, 2\pi]$, then $(\sqrt{R}, T)$ is uniform on $\mathcal{D}$. This transformation was applied to the design of Figure 11, resulting in the design displayed in Figure 12.

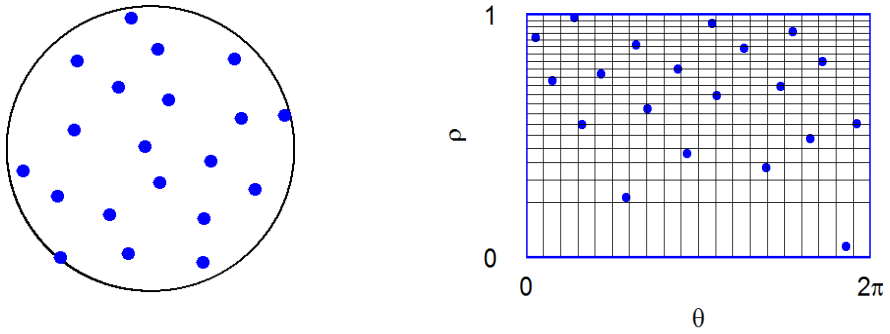

Figure 12: Cartesian (left) and polar (right) representations of the LHD obtained by transforming the maximin LHD of Figure 11 with $\rho \mapsto \sqrt{\rho}$.

5.3. Comparison

The aim of this section is to compare the DoEs presented above with respect to quality criteria, and to evaluate their performance on a set of toy functions. We will denote Dopt1, ..., Dopt4 the D-optimal DoEs for Zernike regression of order N ($1 \leq N \leq 4$) shown in Figure 8, and Spiral-F, Spiral-A, Spiral-G the spiral DoEs (Fermat, Archimede, Galilee) of Figure 9. We also denote PolarLHD the maximin LHD for polar coordinates of Figure 11 and PolarLHD* its transformed version with $\rho \mapsto \sqrt{\rho}$ (Figure 12). All these 20-point DoEs are compared according to the following scheme:

- An assessment is made according to different criteria including the space-filling indicators $\Phi_{\text{Cartesian}}$ and Φ_{Polar} (see Section 5.2), and the D-optimality criterion for the N-order Zernike regression. The latter is given in log-scale via the information matrix M (see [2] for more details);
- A comparison in term of prediction accuracy. The RMSE over a test grid of 1.000 points is computed for the 6 analytical functions shown in Appendix, illustrating various non-linear patterns. For each DoE, the best model is chosen among Zernike polynomials up to order 4, Cartesian GPs and polar GPs with kernels obtained by combination (sum, product, ANOVA) of 1-dimensional kernels as in Section 4.

	D-optimality			maximin criteria	
	$D_{N=2}$	$D_{N=3}$	$D_{N=4}$	Φ_{Polar}	$\Phi_{\text{Cartesian}}$
D-opt1	-159.9	-308.3	-448.3	10.6	3.4
D-opt2	**36.6**	-135.6	-353.1	10.1	3.2
D-opt3	35.4	**49.1**	-18.9	7.4	**2.4**
D-opt4	34.4	47.5	**63.5**	6.3	3.1
Spiral-F	29.7	37.2	44.1	8.8	7.6
Spiral-A	27.2	31.6	32.1	5.2	4.9
Spiral-G	23.3	19.3	-1.4	6.1	4.6
PolarLHD	22.2	20.3	2.4	**3.8**	17.1
PolarLHD*	27.5	32.8	33.0	5.2	3.7

Table 2: Comparison of DoEs according to D-optimality and space-filling criteria.

The results of Table 2 are consistent with the theory of D-optimality and exhibit the lack of robustness of D-optimal designs in case of departure from their assumptions, especially when N is underestimated. The comparison also shows that spiral DoEs have rather good scores for all criteria. The best spirals for Zernike polynomials are the one that have the smaller s (Spiral-F), but the intermediate one (Spiral-A) has the best space-filling scores; It seems to be the best trade-off among spirals. As expected, PolarLHD is interesting for the polar GPs because it optimally fills the polar space, but has the worst space-filling score in Cartesian coordinates (measured by Φ_p). This weaknesses is overcomed by its modified version PolarLHD*, which seems to accomplish the best trade-off for the different criteria among all the DoEs considered.

In Table 3, we see that D-optimal designs of low order $(1, 2)$ have in general poor scores in term of RMSE for the functions considered here, that present non-linearities. Spirals and polarLHDs perform rather well. PolarLHD met our expectations when radial and angular patterns are dominant (functions 1, 2, 3 and 6), and the modified PolarLHD* seems to adapt well to the range of functions and models considered here, confirming its robustness among other DoEs.

6. Discussion and conclusions

We addressed the issue of analyzing costly computer or physical experiments on a disk. Such problems are encountered in various industrial applications, where

	Prediction RMSE (as percentage of the standard deviation)					
	$x\left(x^2-y^2\right)$	$\left(\rho-\frac{1}{4}\right)^2$	$\sin\left(2\pi\rho+\theta\right)$	$\frac{1+\sin(\theta)}{1+\rho^2}$	$\frac{1+x}{1+y^2}$	$\cos\left(3\theta\right)$
D-opt1	14.0	210.1	112.7	75.2	2.9	2.8
D-opt2	14.4	46.6	112.4	60.2	1.7	0.2
D-opt3	0.0	17.5	80.1	18.4	**0.4**	**0.2**
D-opt4	0.0	15.9	82.1	19.0	0.8	1.4
Spiral-F	0.0	0.4	41.2	6.3	0.7	4.5
Spiral-A	0.0	0.1	49.0	4.0	0.7	2.8
Spiral-G	0.0	**0.0**	49.1	8.6	1.3	0.8
PolarLHD	0.0	0.0	42.9	4.5	1.0	0.8
PolarLHD*	0.0	0.3	**35.3**	**3.6**	0.4	2.6

Table 3: Comparison of DoEs in terms of predictive performance on toy functions.

the geometry of the disk is exploited for several technological processes involving rotations or diffusions from the center. For prediction purpose, we introduced so-called polar GP models that take into account the geometry of the disk both in their mean and covariance kernel. The new kernels are defined in polar coordinates. They are obtained as a combination of a kernel for the radius using an Euclidean distance, and a kernel for the angle, based on either chordal or geodesic distances on the unit circle. It was shown on two industrial examples where radial and angular patterns are visible that the approach significantly improves prediction. The best algebraic combination was found to be either a tensor product or a tensor sum, which claims in favor of using a kernel mimicking the more general ANOVA decomposition [13].

In a second time, we considered the problem of designing experiments for circular domains. By introducing a specific distance, we obtained a maximin Latin hypercube for polar coordinates, which is suited to phenomena that have a physical interpretation in polar coordinates. A modified Latin hypercube was proposed for more general situations, with the additional property of filling well the disk. We assessed the performances of these two designs, compared to other common DoEs of the literature, on a set of toy functions aiming at representing various non-linear patterns. As expected, the maximin LHD is outperforming in case of radial or angular patterns, but loses efficiency otherwise. The modified LHD is attractive for its robustness, showing good performances over the whole range of functions and models considered here.

It is important to precise when polar GPs, based on distances on the unit circle, are relevant. One main difference between polar GPs and the usual ones, called here Cartesian GPs, is about the neighborhoods used for prediction. Indeed the prediction

of a GP model is weighting more importantly the observed values corresponding to neighboring locations. For Cartesian GPs, the neighborhoods of a given location correspond to elliptical regions, whereas for geodesic (or chordal) distance, they look like pie chart sectors. This explains why polar GPs give more accurate predictions when there are radial or angular patterns, as may happen for technological processes that involve a rotation or a diffusion from the center. In other situations, involving for instance translations, Cartesian GPs may give better results. These two cases might correspond to the "two clusters of profiles over a circular grid" mentioned by [3] without any additional information about their origin. A knowledge of the process or historical data may help choosing which kernel is appropriate. In any case, there remains a lot of degrees of freedom about a GP model definition, concerning at least the trend shape or the different kernels corresponding to a given distance. To address this problem, aggregation techniques may be a solution.

The discussion above concerning the model choice raises several questions about design of experiments. The study presented in this paper shows the possibility to adapt existing criteria to new distances. In the situations where there is no information about processing, choosing a distance may be difficult, and there is a need for building DoEs that can be suitable for any distance. In such case, a solution would be to consider a multi-criteria approach, for instance by aggregating the maximin criteria in Cartesian and polar coordinates. On the other hand, if a specific kernel is justified, then IMSE-optimal designs could be computed with respect to this kernel.

Appendix: Color representation of test functions

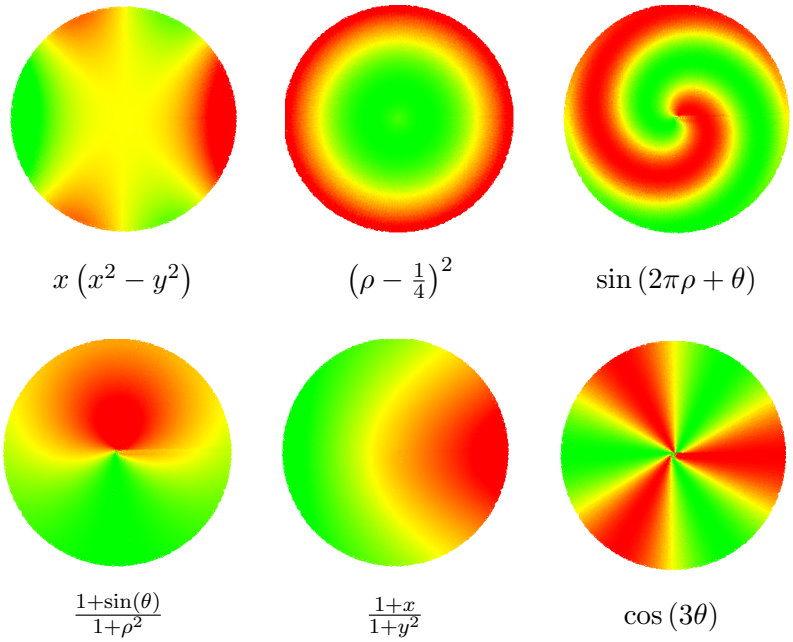

Acknowledgements

The authors would like to thank the company STMicroelectronics for giving the opportunity to work on this research project, and in particular H. Duverneuil. We also thank J. Blue, from Mines Saint-Etienne for useful discussions. Part of this work has been conducted within the frame of the ReDice Consortium, gathering industrial (CEA, EDF, IFPEN, IRSN, Renault) and academic (Ecole des Mines de Saint-Etienne, INRIA, and the University of Bern) partners around advanced methods for Computer Experiments. In particular we would like to thank David Ginsbourger and Nicolas Durrande for their relevant remarks. Some software developments were also facilitated by R packages produced by ReDice and Dice: DiceKriging [22], GPlab [14] and DiceDesign [21].

References

[1] F. Zernike, Diffraction theory of the cut procedure and its improved form, the phase contrast method, Physica 1 (1934) 689–704.

[2] H. Dette, V. Melas, A. Pepelyshev, Optimal Designs for Statistical Analysis with Zernike Polynomials, Technical report: Sonderforschungsbereich Komplexitätsreduktion in Multivariaten Datenstrukturen, Univ., SFB 475, 2006.

[3] G. Pistone, G. Vicario, Kriging prediction from a circular grid: application to wafer diffusion, Applied Stochastic Models in Business and Industry 29 (2013) 350–361.

[4] K. V. Mardia, P. E. Jupp, Directional Statistics, Wiley, 2000.

[5] N. Fisher, Statistical Analysis of Circular Data, Statistical Analysis of Circular Data, Cambridge University Press, 1995.

[6] C. Rasmussen, C. Williams, Gaussian Processes for Machine Learning, The MIT Press, 2006.

[7] G. Jona-Lasinio, A. Gelfand, M. Jona-Lasinio, Spatial Analysis of Wave Direction Data using Wrapped Gaussian Processes, The Annals of Applied Statistics 6 (2012) 1478–1498.

[8] T. Gneiting, Strictly and non-strictly positive definite functions on spheres, Bernoulli 19 (2013) 1327–1349.

[9] E. del Castillo, B. M. Colosimo, S. Tajbakhsh, Geodesic Gaussian Processes for the Parametric Reconstruction of a Free-Form Surface, to appear in Technometrics (2015).

[10] M. D. McKay, R. J. Beckman, W. J. Conover, A comparison of three methods for selecting values of input variables in the analysis of output from a computer code, Technometrics 21 (1979) 239–245.

[11] G. Matheron, Principles of geostatistics, volume 58, Society of Economic Geologists, 1963.

[12] N. Durrande, D. Ginsbourger, O. Roustant, L. Carraro, ANOVA kernels and RKHS of zero mean functions for model-based sensitivity analysis, Journal of Multivariate Analysis 115 (2013) 57–67.

[13] D. Ginsbourger, O. Roustant, D. Schuhmacher, N. Durrande, N. Lenz, On ANOVA decompositions of kernels and Gaussian random field paths, ArXiv e-prints (2014).

[14] Y. Deville, D. Ginsbourger, N. Roustant, O. Contributors: Durrande, GPlab: Laboratory for DiceKriging, 2015. R package version 0.1.0.

[15] M. Batton-Hubert, M. Binois, E. Padonou, Inverse modeling to estimate methane surface emission with optimization and reduced models: application of waste landfill plants, in: 13th Annual Conference of the European Network for Business and Industrial, Ankara, Turkey.

[16] R. Navarro, J. Arines, Complete Modal Representation with Discrete Zernike Polynomials - Critical Sampling in Non Redundant Grids, INTECH Open Access Publisher, 2011.

[17] P. Huber, Robust Statistics, Wiley Series in Probability and Statistics, Wiley-Interscience, 1981.

[18] M. Morris, Gaussian surrogates for computer models with time-varying inputs and outputs, Technometrics 54 (2012) 42–50.

[19] M. Morris, T. Mitchell, Exploratory designs for computational experiments, Journal of Statistical Planning and Inference 43 (1995) 381–402.

[20] G. Damblin, M. Couplet, B. Iooss, Numerical studies of space filling designs: optimization of Latin hypercube samples and subprojection properties, Journal of Simulation 7 (2013) 276–289.

[21] J. Franco, D. Dupuy, O. Roustant, G. Damblin, B. Iooss., DiceDesign: Designs of Computer Experiments, 2014. R package version 1.6.

[22] O. Roustant, D. Ginsbourger, Y. Deville, DiceKriging, DiceOptim: Two R packages for the analysis of computer experiments by kriging-based metamodeling and optimization, Journal of Statistical Software 51 (2012) 1–55.